

# Improved Performance of Polymer Solar Cells by Thermal Evaporation of AgAl Alloy Nanostructures into the Hole-Transport Layer

Jinfeng Wang,<sup>†</sup> Xiangkun Jia,<sup>†</sup> Jianping Zhou,<sup>‡</sup> Likun Pan,<sup>†</sup> Sumei Huang,<sup>†</sup> and Xiaohong Chen<sup>\*,†</sup>

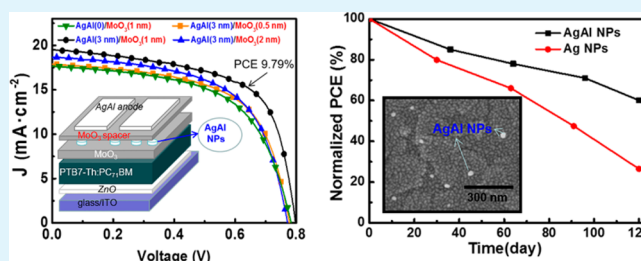
<sup>†</sup>Engineering Research Center for Nanophotonics and Advanced Instrument, Ministry of Education, and School of Physics and Materials Science, East China Normal University, Shanghai 200062, China

<sup>‡</sup>School of Automation Engineering, Shanghai University of Electric Power, Shanghai 200090, China

## S Supporting Information

**ABSTRACT:** The performance characteristics of polymer solar cells (PSCs) incorporated with AgAl and Ag nanostructures and MoO<sub>3</sub> spacer layers were investigated. The power conversion efficiency (PCE) of PSCs is sensitive to the nominal thicknesses of the AgAl nanostructures and the MoO<sub>3</sub> spacer layer. The PCE of a PSC with a 3-nm-thick layer of AgAl nanostructures and a 1-nm-thick MoO<sub>3</sub> isolation layer reached 9.79%, which is higher than the PCE (8.55%) of the reference PSC without metal nanostructures. Compared to PSCs with Ag nanostructures, PSCs with AgAl nanostructures showed better stability and still retained 60% of their initial PCE values after aging for 120 days in air without encapsulation. The enhanced stability of the PSCs is attributed to the formation of AlO<sub>x</sub>, which can inhibit the diffusion of Ag atoms into the neighboring layer. The localized surface plasmonic resonance (LSPR) effect of AgAl nanostructures was retained by inserting an only 1-nm-thick MoO<sub>3</sub> spacer layer between the metal nanostructures and the metal electrode. Our work has demonstrated that using AgAl alloy instead of Ag as plasmonic nanostructures is a better strategy for improving the performance of PSCs, especially in terms of the stability of the cells.

**KEYWORDS:** polymer solar cells, AgAl alloy, local surface plasmonic resonance, metal nanoparticles, stability



## 1. INTRODUCTION

Polymer solar cells (PSCs) have attracted great attention because of their unique advantages, such as solution-processed fabrication, light weights, mechanical flexibility, translucence, and large-scale production at low cost.<sup>1,2</sup> Many approaches have been developed to improve the performance of PSCs, including designing and synthesizing low-band-gap polymers,<sup>3,4</sup> controlling film morphology,<sup>5</sup> inserting an optical spacer layer, using surface plasmonic effects to boost the light absorption, and engineering the interface to enhance the charge collection efficiency.<sup>6,7</sup> The representative high-efficiency inverted bulk heterojunction PSCs based on poly[4,8-bis(5-(2-ethylhexyl)thiophen-2-yl)-benzo[1,2-*b*:4,5-*b'*]dithiophene-*alt*-3-fluorothieno [3,4-*b*]thiophene-2-carboxylate] (PTB7-Th) and [6,6]-phenyl-C<sub>71</sub>-butyric acid methyl ester (PC<sub>71</sub>BM) blend systems have reached power conversion efficiencies (PCEs) of ~8–10% through the introduction of polyelectrolytes,<sup>8,9</sup> fullerene-derivative-doped ZnO and InZnO,<sup>10,11</sup> LiF-modified ZnO,<sup>12,13</sup> and ionic-liquid-functionalized carbon nanoparticles<sup>14–16</sup> as electrode interlayers. Although the novel low-band-gap polymers extend spectral absorption, their intrinsic disadvantages of short exciton diffusion lengths and low carrier mobilities still limit the photoactive layer thickness and inhibit further enhancement of the PCEs of PSCs. Therefore,

improving the light absorption of the limited-thickness photoactive layer triggers the emergence of light-trapping techniques, such as optical spacer layers, diffraction gratings, tandem structures, and plasmonic nanostructures.<sup>17,18</sup>

Enhanced optical absorption has been demonstrated for PSCs incorporating metal nanostructures because of their enhanced near-field and forward light scattering caused by plasmonic effects.<sup>19–21</sup> In previous reports, metal nanostructures have usually been incorporated into the buffer and photoactive layers<sup>22–25</sup> and inserted between tandem cells.<sup>18</sup> The plasmonic effects have been shown to be partly responsible for the enhancement of the PCEs of PSCs with incorporated metal nanostructures. Meanwhile, the improved electrical conductivities of buffer and photoactive layers incorporated with metal nanostructures are considered to be important factors in enhancing the PCEs of PSCs. However, some reports have shown deteriorating performances for PSCs made with metal nanostructures because incorporating metal nanostructures increases the interfacial barrier and induces carrier traps and carrier recombination.<sup>26,27</sup> Therefore, metal nanoparticles

Received: August 13, 2016

Accepted: September 13, 2016

Published: September 13, 2016

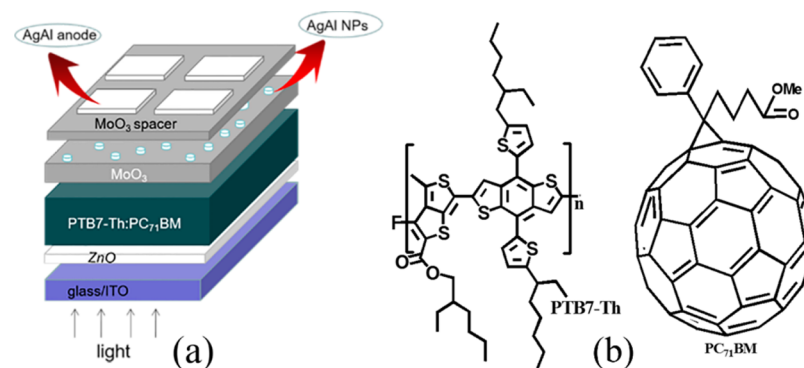


**Figure 1.** (a) PSC device structure. (b) Molecular structures of PTB7-Th and PC<sub>71</sub>BM.

(NPs) incorporated into the photoactive layer usually need be coated with an insulating layer such as SiO<sub>2</sub> to limit the carrier traps and/or recombination.<sup>22</sup> Metal nanostructures inserted into the buffer layer help to inhibit metal-NP-induced carrier recombination and reduce the serial resistance of cells. Furthermore, optimal carrier collecting/transporting layers are very important for the enhanced performance of PSCs with metal NPs to inhibit defects in the photoactive layers from penetrating into the overall PSCs.

The plasmonic effects of metal NPs are characteristic of the type of metal used and are related to the morphologies, sizes, and arrangements of NPs, as well as the surrounding medium.<sup>28,29</sup> Metal nanostructures formed by a simple thermal evaporation technique show wider resonance wavelength ranges than solution-synthesized metal NPs, which can increase the absorption of the photoactive layer.<sup>30</sup> The metal nanostructures are thermally evaporated onto the rear side of the photoactive layer, which can inhibit the destructive interference due to the Fano resonance effect and weaken light loss caused by the self-absorption of metal nanostructures.<sup>31,32</sup> Our previous reports have shown that PSCs with Au nanostructures thermally evaporated onto the rear side of the photoactive layer as a modified cathode improved the efficiency by 20–30%, showing obvious plasmon enhancement of the PSCs.<sup>33</sup> Yao et al.<sup>34</sup> further evaporated Ag and/or Au NPs in the WO<sub>3</sub> anode buffer layer in inverted PSCs, which led to an obvious improvement in the PCE from ~4.6% to ~6.6%. Metal nanostructures inserted into the WO<sub>3</sub> layer can efficiently reduce metal-NP-induced carrier recombination by isolating NPs from the photoactive layer.<sup>34,35</sup> However, Ag and Au atoms typically diffuse easily into the photoactive layer during thermal evaporation and aging, which can accelerate the deterioration of cells.<sup>12,13,36</sup> AgAl alloy electrodes have been demonstrated to prevent the diffusion of Ag atoms into the photoactive layer through the formation of the interfacial AlO<sub>x</sub>.<sup>37,38</sup> In this work, the performance of plasmonic PSCs with AgAl nanostructures inserted into the MoO<sub>3</sub> anode buffer layer was investigated. MoO<sub>3</sub>, as an anode interlayer, has been demonstrated to form ohmic contacts with numerous organic hole-transporting materials and air-stable high-work-function metals in PSCs.<sup>12,39</sup> MoO<sub>3</sub> as a dielectric material is expected to inhibit the dissipation of plasmon resonance by isolating the metal electrode.<sup>33</sup> Furthermore, its high conductivity compared to that of the insulating material helps to allow the flexible choice of the thicknesses of the isolation layer and hole-transport film and can improve the carrier-transport and -collection abilities. It was found that the plasmonic effects of AgAl nanostructures in PSCs can be retained by inserting a

MoO<sub>3</sub> isolation layer of only 1-nm thickness between the metal nanostructures and the metal electrode. An enhancement of the PCEs of PSCs with AgAl nanostructures was observed, compared to that of reference PSCs without plasmonic properties. Furthermore, PSCs with AgAl compared to pure Ag nanostructures showed better stability, indicating that use AgAl alloy in plasmonic nanostructures helps to improve the stability of plasmonic PSCs.

## 2. EXPERIMENTAL SECTION

PSCs with a structure of ITO/ZnO/PTB7-Th:PC<sub>71</sub>BM/MoO<sub>3</sub>/metal nanostructures/MoO<sub>3</sub>/metal electrode using Ag and AgAl alloy for the metal nanostructures were fabricated as shown in Figure 1. Pre-cleaned indium tin oxide (ITO)/glass substrates (10 Ω/□) were treated with ultraviolet ozone for 25 min, and then sol-gel ZnO solutions were spin-coated at 4000 rpm for 60 s onto the ITO to form 20-nm films, which were then annealed at 150 °C for 30 min in air. The sol-gel ZnO NPs were synthesized following the procedures described in previous reports.<sup>12,13</sup> In a typical synthesis, a stoichiometric amount of tetramethylammonium hydroxide dissolved in ethanol (0.5 M) was gradually dropped into 0.1 M zinc acetate dihydrate dissolved in dimethyl sulfoxide (DMSO), and the mixture was stirred for 1 h at room temperature. After being washed with hexane/ethanol (2:1) mixed solvent, the ZnO NPs were dispersed in ethanol. The weight ratio (wt %) of Al to Ag in the AgAl alloy, purchased from Trillion Metals Co., Ltd. (Beijing, China), was 3 wt %. PC<sub>71</sub>BM (99.5%) was purchased from Solenne BV, and PTB7-Th (99%) was purchased from 1-Material Inc. The molecular structures of PTB7-Th and PC<sub>71</sub>BM are shown in Figure 1. Solutions containing PTB7-Th and PC<sub>71</sub>BM in a 1:1.5 weight ratio dissolved in chlorobenzene/1,8-dioctane (97:3, v/v) were spin-coated in an argon-filled glovebox on top of the ZnO films to form 80-nm-thick photoactive films. Finally, an 8-nm MoO<sub>3</sub> hole-transport layer, a layer of AgAl alloy or Ag nanostructures with different nominal thicknesses, a MoO<sub>3</sub> spacer layer, and a 100-nm AgAl or Ag metal electrode were successively evaporated onto the PTB7-Th:PC<sub>71</sub>BM photoactive layer at a base pressure of 5 × 10<sup>-4</sup> Pa. The deposition rate was monitored with a quartz-oscillating thickness monitor. The active area of the devices was 0.1 cm<sup>2</sup>. The resulting PSCs were stored in air in a chamber at 10% relative humidity.

The *J*-*V* characteristics of the PSCs were measured with a Keithley 2440 SourceMeter together with a Newport solar simulator with an AM1.5G illumination of 100 mW/cm<sup>2</sup> calibrated with a standard silicon reference cell. The incident-photon-to-current conversion efficiencies (IPCEs) of the PSCs was measured over the wavelength range from 300 to 800 nm using a Newport Optical Power Meter 2936-R and recorded using TracQ Basic software. The dark *J*-*V* characteristics of the cells were measured using an electrochemical workstation (AUTOLAB PGSTAT302N). The absorption and reflectivity spectra of the samples were measured using a UV/vis spectrophotometer (Hitachi U-3900). The surface morphologies of samples were investigated by field-emission scanning electron microscopy (FESEM, Hitachi S-4800).

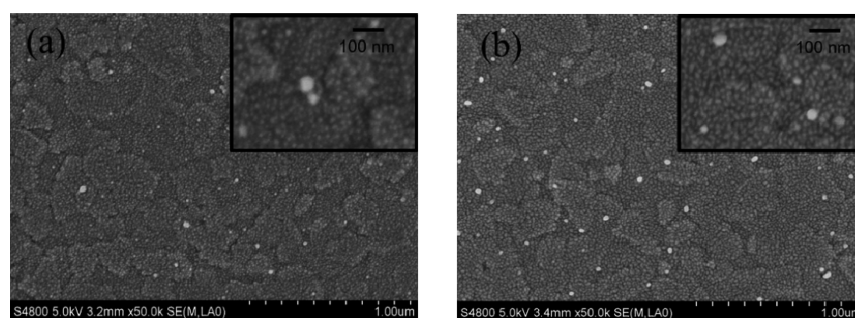


Figure 2. SEM images of (a) AgAl and (b) Ag nanostructures with 3-nm nominal thickness evaporated on top of the glass/MoO<sub>3</sub> surface.

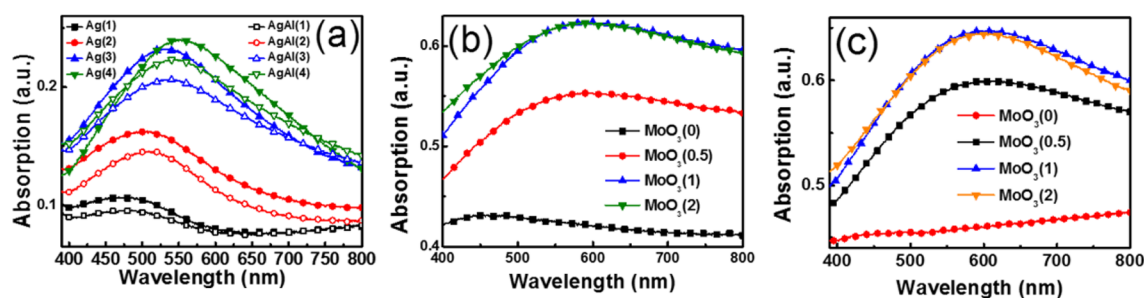


Figure 3. (a) Absorption spectra of AgAl and Ag nanostructures with different nominal thicknesses evaporated on top of glass/MoO<sub>3</sub>(8) substrates. (b,c) Absorption spectra of (b) AgAl and (c) Ag nanostructures with 3-nm nominal thickness inserted with different-thickness MoO<sub>3</sub> spacer layers between the Al electrode and the metal nanostructures, where the structure of the samples was MoO<sub>3</sub>(8)/metal(3)/MoO<sub>3</sub>(x)/Al(10). The numbers in parentheses indicate the average layer thicknesses in nanometers.

### 3. RESULTS AND DISCUSSION

Ag and AgAl films with a 3-nm nominal thickness were thermally evaporated onto an 8-nm-thick MoO<sub>3</sub> film surface. White island-shaped nanostructures of Ag and AgAl clearly formed because of the high conductivity of the metals, as shown in Figure 2. The sizes of the Ag and AgAl island nanostructures were not very uniform because the island nanostructures were formed by the aggregation of Ag atoms during thermal evaporation. The sizes of most of the metal island nanostructures were about 20–50 nm. Continuous structures of Ag and AgAl films could not be formed because of the self-aggregation effects of metal films, which is consistent with a previous report.<sup>40</sup> Ag and AgAl island-shaped nanostructures of different sizes were distributed onto the MoO<sub>3</sub> film surface, and these Ag and AgAl nanostructures would produce localized surface plasmon resonance (LSPR) effects in the solar cells.

To explore the LSPR effects of Ag and AgAl alloy island-shaped nanostructures, the absorption spectra of the Ag and AgAl nanostructures were recorded. Figure 3a shows the absorption spectra of Ag and AgAl nanostructures with different nominal thicknesses. In Figure 3a, the Ag and AgAl nanostructures thermally evaporated onto an 8-nm-thick MoO<sub>3</sub> film are not covered by evaporating MoO<sub>3</sub> layer. The plasmon resonance wavelength of metallic nanoparticles is sensitive to the sizes, shapes, and arrangements of nanoparticles, as well as the surrounding environment. The sizes of the Ag and AgAl island-shaped nanostructures became larger as the nominal thickness was increased from 1 to 4 nm. Furthermore, the interactions between plasmons from individual metal islands increased as their separation was reduced.<sup>33</sup> Therefore, the red shift of the absorption of the pure metal or alloy with increasing thickness (Figure 3a) is caused by the larger sizes of the metal island-shaped nanostructures and the stronger plasmon interactions between the metal islands. The

similar absorption spectra of both the pure and alloyed metals show that the LSPR effects of AgAl nanostructures are almost the same as those of Ag nanostructures, indicating that the slight doping with Al has not obviously changed the LSPR behavior of the Ag metal. Figure 3b,c shows the absorption spectra of AgAl and Ag nanostructures simulating the solar-cell environment. The Ag and AgAl electrodes were used in the realized solar cells, as shown in Figure 1. A 10-nm-thick Al electrode instead of a Ag or AgAl electrode was evaporated onto the spacer of MoO<sub>3</sub> in the simulated structure to avoid the SPR effects of Ag or AgAl films. The absorption peaks of the AgAl and Ag nanostructures covered with a MoO<sub>3</sub> spacer layer were further red-shifted to 600 from 540 nm because the LSPR effects of metal nanoparticles are sensitive to the surrounding environment.<sup>33</sup> The LSPR effects of the Ag and AgAl nanostructures almost disappeared when the Al electrode was directly evaporated onto the Ag and AgAl films without the insertion of a MoO<sub>3</sub> isolation layer. The absorption intensities of the Ag and AgAl nanostructures obviously increased upon insertion of a 0.5-nm-thick MoO<sub>3</sub> spacer layer and were almost completely recovered with a 1-nm-thick MoO<sub>3</sub> isolation layer. This indicates that a MoO<sub>3</sub> spacer layer with a 1-nm thickness can obviously inhibit the dissipation of the LSPR energy of Ag and AgAl nanostructures through the top metal electrode.

To investigate the effects of incorporating plasmonic structures into the MoO<sub>3</sub> hole-transport layer on the PCEs of PSCs, we fabricated sets of seven types of cells. Figure 4 shows typical *J*–*V* curves of PSCs AgAl nanostructures incorporated in the MoO<sub>3</sub> layer. The average parameters and standard deviations of these devices are summarized in Table 1. The highest PCE of the cells with a structure of MoO<sub>3</sub>(8)/AgAl(3)/MoO<sub>3</sub>(1) reached 9.79%, which is 14.5% larger than the PCE (8.55%) of the corresponding reference cell without AgAl nanostructures. The serial resistance (*R*<sub>s</sub>) values of PSCs with a

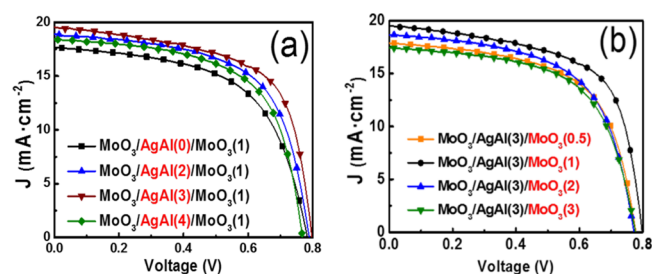


**Figure 4.**  $J$ - $V$  curves of PSCs incorporated with (a) AgAl nanostructures with different nominal thicknesses and (b) 3-nm-thick layer of AgAl nanostructures isolated with different-thickness  $\text{MoO}_3$  spacer layers, where the anode structure of the PSCs was  $\text{MoO}_3(8)/\text{AgAl}$  nanostructures( $x$ )/ $\text{MoO}_3(y)/\text{AgAl}(100)$  electrode. The numbers in parentheses indicate the average layer thicknesses in nanometers.

layer of AgAl nanostructures with a nominal thickness of 3 nm gradually increased to 52.1 from 38.5  $\Omega\cdot\text{cm}^2$  as the thickness of the  $\text{MoO}_3$  spacer layer was increased to 3 from 1 nm, as shown in Figure 4b. The similar range of the open-circuit voltages ( $V_{oc}$ ) of different PSCs indicates that their built-in electrical fields still remained stable after the insertion of AgAl nanostructures.<sup>34</sup> The slightly larger fill factor (FF) value and lower  $R_s$  value of the PSCs with the structure  $\text{MoO}_3(8)/\text{AgAl}(3)/\text{MoO}_3(1)$  indicate enhanced hole-transport and -collection abilities, which help to improve the photocurrent of the PSC with 3-nm AgAl nanostructures, indicating that a thicker  $\text{MoO}_3$  isolation layer can inhibit the carrier-transport and -collection abilities. The same trends can also be observed in the PSCs with Ag nanostructures, as shown in Figure S1 and Table S1. The best PSC with the structure  $\text{MoO}_3(8)/\text{Ag}(3)/\text{MoO}_3(1)$  reached a PCE of 9.28%, which is significantly higher than the PCE (7.89%) of the PSC with a 3-nm-thick  $\text{MoO}_3$  spacer layer. These results show that a proper thickness of the  $\text{MoO}_3$  isolation layer is important for obtaining highly efficient PSCs.

Figure 5a shows the IPCE curves of PSCs with and without metal nanostructures. The photocurrent in the range from 500 to 700 nm, where the LSPR of AgAl and Ag nanostructures is strong (cf. Figure 3), is substantially increased in the cells with AgAl and Ag incorporated into the  $\text{MoO}_3$  layer. This can be even more clearly observed by plotting the normalized IPCE as a function wavelength, where the IPCE is normalized with respect to that of the corresponding device without metal nanostructures, as shown in Figure 5b. These relative curves roughly match the absorption spectrum profiles of the  $\text{MoO}_3/\text{AgAl}$  (or Ag) nanostructures/ $\text{MoO}_3/\text{Al}$  films and provide strong evidence that the LSPR effects of AgAl and Ag nanostructures can really induce improvements in the PCEs

of PSCs.<sup>33</sup> However, the average value of the enhancement factor obtained from the extracted absorption is obviously lower than that of the IPCE enhancement factor, as shown in Figure 5c. This indicates that the enhanced IPCE is partly attributable to the plasmonic enhanced absorption. Other factors such as improved carrier-transport and -collection abilities might also contribute to the enhanced IPCE.<sup>41</sup>

To further understand the mechanism responsible for the enhanced performances of solar cells with AgAl nanostructures, we determined the maximum exciton generation rates ( $G_{\text{max}}$ ) and exciton dissociation probabilities [ $P(E,T)$ ] of the PSCs.<sup>41,42</sup> Figure 6a shows the effects of metal nanostructures on the photocurrent density ( $J_{\text{ph}}$ ) of the cells.  $J_{\text{ph}}$  is defined as  $J_{\text{ph}} = J_L - J_D$ , where  $J_L$  and  $J_D$  are the current densities under illumination and in the dark, respectively.  $V_{\text{eff}}$  is determined as  $V_{\text{eff}} = V_0 - V_a$ , where  $V_0$  is the voltage at which  $J_{\text{ph}} = 0$  and  $V_a$  is the applied bias voltage.  $J_{\text{ph}}$  was found to increase linearly with  $V_{\text{eff}}$  in the low- $V_{\text{eff}}$  range and to saturate gradually at high  $V_{\text{eff}}$ . Generally, the saturated photocurrent ( $J_{\text{sat}}$ ) is correlated with the maximum exciton generation rate ( $G_{\text{max}}$ ), exciton dissociation probability, and carrier-transport and -collection probabilities in the high- $V_{\text{eff}}$  range.  $G_{\text{max}}$  can be calculated from  $J_{\text{ph}} = qG_{\text{max}}L$ , where  $q$  is the electronic charge and  $L$  is the thickness of the active layer (80 nm). The values of  $G_{\text{max}}$  for the control device and device with AgAl nanostructures are  $1.49 \times 10^{28} \text{ m}^{-3}\text{s}^{-1}$  ( $J_{\text{sat}} = 191 \text{ A/m}^2$ ) and  $1.74 \times 10^{28} \text{ m}^{-3}\text{s}^{-1}$  ( $J_{\text{sat}} = 223 \text{ A/m}^2$ ), respectively. An impressive enhancement of  $G_{\text{max}}$  occurred after the incorporation of AgAl nanostructures. Because  $G_{\text{max}}$  is mainly governed by the absorption of light in the active layer, the enhanced  $G_{\text{max}}$  suggests increased light absorption in the device with AgAl nanostructures. Considering the constant of absorbed incident photons for one cell, assuming that all of the photogenerated excitons are dissociated into free charge carriers in the high- $V_{\text{eff}}$  range,  $J_{\text{sat}}$  is then limited by the carrier transport and collection.  $P(E,T)$  can be obtained from the ratio of  $J_{\text{ph}}/J_{\text{sat}}$ . The  $P(E,T)$  value of the cells with  $\text{MoO}_3(8)/\text{AgAl}(3)/\text{MoO}_3(1)$  increased to 94.5% from the 92.1% obtained for the control cells, indicating that the AgAl nanostructures probably benefit the dissociation of excitons into free charge carriers and improve the carrier-transport and -collection probabilities. However, the  $P(E,T)$  values of cells with AgAl nanostructures was decreased to 91.6% using a 3-nm-thick  $\text{MoO}_3$  isolation layer, indicating that thicker  $\text{MoO}_3$  layer can inhibit the carrier-transport and -collection probabilities in PSCs.

Figure 6b shows the normalized PCEs of PSCs as a function of aging time. The devices without encapsulation were kept in a drying cabinet with a relative humidity of 10% under ambient atmosphere. The reference PSCs with AgAl and Ag electrodes exhibited better stability than the PSCs with plasmonic structures. The PSCs with Ag and AgAl nanostructures retained

**Table 1.** Parameters of PSCs Incorporated with AgAl Nanostructures Isolated with  $\text{MoO}_3$  Spacer Layers

$\text{MoO}_3/\text{AgAl}/\text{MoO}_3$ layer thicknesses (nm)	$V_{oc}$ (V)	$J_{sc}$ ( $\text{mA}/\text{cm}^2$ )	FF (%)	PCE (%)	$R_s$ ( $\Omega\cdot\text{cm}^2$ )
8/0/1	$0.78 \pm 0.01$	$17.9 \pm 0.3$	$59.8 \pm 0.4$	$8.45 \pm 0.10$	47.5
8/2/1	$0.78 \pm 0.01$	$18.5 \pm 0.3$	$61.5 \pm 0.9$	$9.03 \pm 0.20$	36.3
8/3/1	$0.78 \pm 0.01$	$19.6 \pm 0.2$	$61.9 \pm 0.7$	$9.69 \pm 0.10$	38.5
8/4/1	$0.78 \pm 0.01$	$18.2 \pm 0.6$	$61.2 \pm 1.0$	$8.59 \pm 0.10$	40.2
8/3/0.5	$0.78 \pm 0.01$	$18.1 \pm 0.3$	$60.2 \pm 0.4$	$8.41 \pm 0.10$	42.8
8/3/2	$0.78 \pm 0.01$	$18.9 \pm 0.4$	$59.6 \pm 1.2$	$8.58 \pm 0.10$	45.2
8/3/3	$0.78 \pm 0.01$	$17.3 \pm 0.4$	$56.0 \pm 0.5$	$7.39 \pm 0.20$	52.1

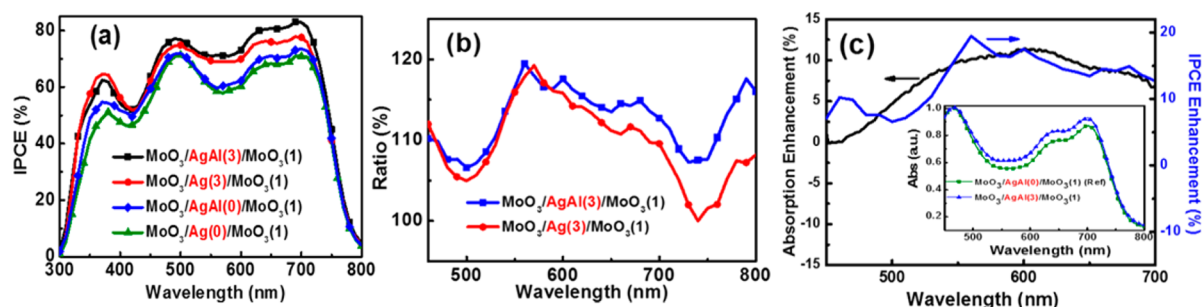


**Figure 5.** (a) IPCE curves of PSCs with and without metal nanostructures. (b) Normalized IPCE values vs wavelength, where each IPCE value was normalized with respect to that of the corresponding reference device without metal nanostructures. Specifically, the curves show the IPCE values for the devices MoO<sub>3</sub>(8)/AgAl(3)/MoO<sub>3</sub>(1) and MoO<sub>3</sub>(8)/Ag(3)/MoO<sub>3</sub>(1) divided by those of the reference device MoO<sub>3</sub>(8)/MoO<sub>3</sub>(1). (c) Comparison of enhanced IPCEs of AgAl-nanostructure-based cells with absorption variations: (right) IPCE enhancement factors,  $\Delta\text{IPCE}/\text{IPCE}_{\text{ref}}$  ( $\Delta\text{IPCE} = \text{IPCE}_{\text{plasmonic}} - \text{IPCE}_{\text{ref}}$ ), (left) absorption enhancement factors,  $\Delta\text{Abs}/\text{Abs}_{\text{ref}}$  ( $\Delta\text{Abs} = \text{Abs}_{\text{plasmonic}} - \text{Abs}_{\text{ref}}$ ). Inset: Absorption spectra of cells with and without AgAl nanostructures. The numbers in parentheses indicate the average layer thicknesses in nanometers.

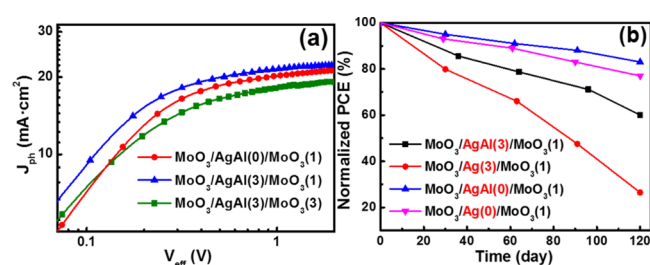


**Figure 6.** (a)  $J_{\text{ph}}-V_{\text{eff}}$  characteristics measured for PSCs with different device structures. (b) Normalized PCEs of PSCs with and without metal nanostructures as a function of aging time. The numbers in parentheses indicate the average layer thicknesses in nanometers.

26% and 60%, respectively, of the initial PCE values after 120 days of aging, indicating that AgAl nanostructures have advantages over Ag nanostructures for improving the performance and stability of PSCs.

To explain the reason for the enhanced stability of cells with AgAl nanostructures, the dark  $J-V$  characteristics of the PSCs were investigated. Figure 7 shows the dark  $J-V$  characteristic

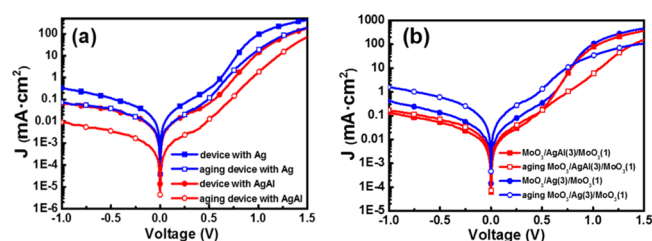


**Figure 7.** Dark  $J-V$  curves of PSCs (a) without and (b) with incorporated metal nanostructures in the initial stage and after aging for 14 days. The numbers in parentheses indicate the average layer thicknesses in nanometers.

curves of different types of cells. The reverse leakage currents of PSCs with metal nanostructures were increased compared to those of the reference PSCs without metal nanostructures. The PSCs with AgAl compared to Ag nanostructures exhibited better diode characteristics with a lower leakage current and a higher rectification ratio anode. Compared to the initial dark  $J-V$  characteristics, the reverse dark currents of PSCs with Ag nanostructures compared to AgAl nanostructures are significantly increased after 14 days of aging, indicating that PSCs with Ag compared to AgAl nanostructures more easily

deteriorate during aging. Solar cells with AgAl alloy electrodes in our previous report<sup>12</sup> were demonstrated to prevent the diffusion of Ag atoms into the photoactive layer through the formation of interfacial AlO<sub>x</sub> during thermal evaporation and aging, which improved the stability of the resulting cells.<sup>12,37</sup> Similarly, PSCs with AgAl nanostructures compared to Ag nanostructures showed better stability, as shown in Figure 6b, because of AlO<sub>x</sub> formation in the AgAl nanostructures.<sup>12,43</sup> However, the island-shaped AgAl and Ag nanostructures with small sizes exhibited much larger surface energies than AgAl and Ag electrode films,<sup>44</sup> which allow Ag atoms in nanostructures to more easily diffuse into the adjacent layer.<sup>36</sup> Therefore, PSCs incorporated with metal nanostructures show inferior stability compared to the reference PSCs without metal nanostructures, which limits the function of metal nanoparticles in cells. Metal alloys such as AgAl nanostructures provide a potential choice to improve the performance of PSCs, especially in terms of the stability of the cells.

#### 4. CONCLUSIONS

In summary, the plasmonic performance characteristics of PSCs with AgAl and Ag nanostructures inserted into MoO<sub>3</sub> hole-transport layer were investigated. The PCEs of PSCs incorporated with metal nanostructures isolated with the right thickness of MoO<sub>3</sub> spacer layer obviously improved compared to PSCs without metal nanostructures. The stability of PSCs incorporated with metal nanostructures is deteriorated compared to that of the reference PSCs without metal nanostructures. However, the stability of PSCs with AgAl instead of pure Ag nanostructures is significantly improved, indicating that use of AgAl alloy for the plasmonic nanostructures helps to improve the stability of plasmonic PSCs because of the formation of AlO<sub>x</sub>. The strategy of using a metal alloy such as AgAl nanostructures as plasmonic structures for PSCs can be expected to improve the performance of PSCs, especially in terms of the stability of the cells.

#### ■ ASSOCIATED CONTENT

##### Supporting Information

The Supporting Information is available free of charge on the ACS publications Web site at The Supporting Information is available free of charge on the ACS Publications website at DOI: 10.1021/acsami.6b10173.

$J-V$  curves and parameters of PSCs with and without Ag nanostructures (PDF)

## AUTHOR INFORMATION

## Corresponding Author

\*E-mail: [xhchen@phy.ecnu.edu.cn](mailto:xhchen@phy.ecnu.edu.cn). Tel.: +86 21 62233676. Fax: +86 21 62234321.

## Notes

The authors declare no competing financial interest.

## ACKNOWLEDGMENTS

This work was supported by the National Natural Science Foundation of China (Grants 61275038 and 11274119).

## REFERENCES

- (1) Chen, H.-Y.; Hou, J.; Zhang, S.; Liang, Y.; Yang, G.; Yang, Y.; Yu, L.; Wu, Y.; Li, G. Polymer Solar Cells with Enhanced Open-circuit Voltage and Efficiency. *Nat. Photonics* **2009**, *3*, 649–653.
- (2) Park, S. H.; Roy, A.; Beaupre, S.; Cho, S.; Coates, N.; Moon, J. S.; Moses, D.; Leclerc, M.; Lee, K.; Heeger, A. J. Bulk Heterojunction Solar Cells with Internal Quantum Efficiency Approaching 100%. *Nat. Photonics* **2009**, *3*, 297–302.
- (3) Jo, J.; Na, S. I.; Kim, S. S.; Lee, T. W.; Chung, Y.; Kang, S. J.; Vak, D.; Kim, D. Y. Three-Dimensional Bulk Heterojunction Morphology for Achieving High Internal Quantum Efficiency in Polymer Solar Cells. *Adv. Funct. Mater.* **2009**, *19*, 2398–2406.
- (4) Dou, L. T.; Chang, W. H.; Gao, J.; Chen, C. C.; You, J. B.; Yang, Y. A Selenium-Substituted Low-Bandgap Polymer with Versatile Photovoltaic Applications. *Adv. Mater.* **2013**, *25*, 825–831.
- (5) Ye, L.; Zhang, S.; Ma, W.; Fan, B.; Guo, X.; Huang, Y.; Ade, H.; Hou, J. From Binary to Ternary Solvent: Morphology Fine-Tuning of D/A Blends in PDPP3T-Based Polymer Solar Cells. *Adv. Mater.* **2012**, *24* (47), 6335–6341.
- (6) He, Z. C.; Zhong, C. M.; Huang, X.; Wong, W. Y.; Wu, H. B.; Chen, L. W.; Su, S. J.; Cao, Y. Simultaneous Enhancement of Open-Circuit Voltage, Short-Circuit Current Density, and Fill Factor in Polymer Solar Cells. *Adv. Mater.* **2011**, *23*, 4636–4643.
- (7) Roy, A.; Park, S. H.; Cowan, S.; Tong, M. H.; Cho, S. N.; Lee, K.; Heeger, A. J. Titanium Suboxide as an Optical Spacer in Polymer Solar Cells. *Appl. Phys. Lett.* **2009**, *95* (1), 013302.
- (8) Seo, J. H.; Gutacker, A.; Sun, Y.; Wu, H.; Huang, F.; Cao, Y.; Scherf, U.; Heeger, A. J.; Bazan, G. C. Improved High-efficiency Organic Solar Cells via Incorporation of a Conjugated Polyelectrolyte Interlayer. *J. Am. Chem. Soc.* **2011**, *133* (22), 8416–8419.
- (9) Yang, T.; Wang, M.; Duan, C.; Hu, X.; Huang, L.; Peng, J.; Huang, F.; Gong, X. Inverted Polymer Solar Cells with 8.4% Efficiency by Conjugated Polyelectrolyte. *Energy Environ. Sci.* **2012**, *5* (8), 8208–8214.
- (10) Liao, S. H.; Jhuo, H. J.; Cheng, Y. S.; Chen, S. A. Fullerene Derivative-Doped Zinc Oxide Nanofilm as the Cathode of Inverted Polymer Solar Cells with Low-Bandgap Polymer (PTB7-Th) for High Performance. *Adv. Mater.* **2013**, *25* (34), 4766–4771.
- (11) Liao, S.-H.; Jhuo, H.-J.; Yeh, P.-N.; Cheng, Y.-S.; Li, Y.-L.; Lee, Y.-H.; Sharma, S.; Chen, S.-A. Single Junction Inverted Polymer Solar Cell Reaching Power Conversion Efficiency 10.31% by Employing Dual-doped Zinc Oxide Nano-film as Cathode Interlayer. *Sci. Rep.* **2014**, *4*, 6813.
- (12) Jia, X.; Jiang, Z.; Chen, X.; Zhou, J.; Pan, L.; Zhu, F.; Sun, Z.; Huang, S. Highly Efficient and Air Stable Inverted Polymer Solar Cells using LiF-Modified ITO Cathode and MoO<sub>3</sub>/AgAl Alloy Anode. *ACS Appl. Mater. Interfaces* **2016**, *8* (6), 3792–3799.
- (13) Lu, Z.; Chen, X.; Zhou, J.; Jiang, Z.; Huang, S.; Zhu, F.; Piao, X.; Sun, Z. Performance Enhancement in Inverted Polymer Solar Cells Incorporating Ultrathin Au and LiF Modified ZnO Electron Transporting Interlayer. *Org. Electron.* **2015**, *17*, 364–370.
- (14) Chen, X.; Yang, J.; Haley, L. Y. X. C.; Lu, J.; Zhu, F.; Loh, K. P. Towards High Efficiency Solution Processable Inverted Bulk Heterojunction Polymer Solar Cells Using Modified Indium Tin Oxide Cathode. *Org. Electron.* **2010**, *11* (12), 1942–1946.
- (15) Zhu, F.; Chen, X.; Zhou, L.; Zhou, J.; Yang, J.; Huang, S.; Sun, Z. Dependence of the Performance of Inverted Polymer Solar Cells on Thickness of an Electron Selective ZnO Layer Deposited by Magnetron Sputtering. *Thin Solid Films* **2014**, *551*, 131–135.
- (16) Zhu, F.; Chen, X.; Lu, Z.; Yang, J.; Huang, S.; Sun, Z. Efficiency Enhancement of Inverted Polymer Solar Cells Using Ionic Liquid-Functionalized Carbon Nanoparticles-Modified ZnO as Electron Selective Layer. *Nano-Micro Lett.* **2014**, *6* (1), 24–29.
- (17) Park, H. J.; Xu, T.; Lee, J. Y.; Ledbetter, A.; Guo, L. J. Photonic Color Filters Integrated with Organic Solar Cells for Energy Harvesting. *ACS Nano* **2011**, *5* (9), 7055–7060.
- (18) Ran, N. A.; Love, J. A.; Takacs, C. J.; Sadhanala, A.; Beavers, J. K.; Collins, S. D.; Huang, Y.; Wang, M.; Friend, R. H.; Bazan, G. C.; Nguyen, T.-Q. Harvesting the Full Potential of Photons with Organic Solar Cells. *Adv. Mater.* **2016**, *28* (7), 1482–1488.
- (19) Li, X.; Ren, X.; Xie, F.; Zhang, Y.; Xu, T.; Wei, B.; Choy, W. C. High-Performance Organic Solar Cells with Broadband Absorption Enhancement and Reliable Reproducibility Enabled by Collective Plasmonic Effects. *Adv. Opt. Mater.* **2015**, *3* (9), 1220–1231.
- (20) Pors, A.; Nielsen, M. G.; Bernardini, T.; Weeber, J.-C.; Bozhevolnyi, S. I. Efficient Unidirectional Polarization-Controlled Excitation of Surface Plasmon Polaritons. *Light: Sci. Appl.* **2014**, *3*, e197.
- (21) Yao, M.; Jia, X.; Liu, Y.; Guo, W.; Shen, L.; Ruan, S. Surface Plasmon Resonance Enhanced Polymer Solar Cells by Thermally Evaporating Au into Buffer Layer. *ACS Appl. Mater. Interfaces* **2015**, *7* (33), 18866–18871.
- (22) Li, X.; Choy, W. C. H.; Lu, H.; Sha, W. E.; Ho, A. H. P. Efficiency Enhancement of Organic Solar Cells by Using Shape-Dependent Broadband Plasmonic Absorption in Metallic Nanoparticles. *Adv. Funct. Mater.* **2013**, *23* (21), 2728–2735.
- (23) Yuan, K.; Chen, L.; Chen, Y. W. In Situ Photocatalytically Heterostructured ZnOAg Nanoparticle Composites as Effective Cathode-Modifying Layers for Air-Processed Polymer Solar Cells. *Chem. - Eur. J.* **2015**, *21*, 11899–11906.
- (24) Yuan, K.; Chen, L.; Chen, Y. Versatile Electron-collecting Interfacial Layer by in Situ Growth of Silver Nanoparticles in Nonconjugated Polyelectrolyte Aqueous Solution for Polymer Solar Cells. *J. Phys. Chem. B* **2014**, *118*, 11563–11572.
- (25) Yuan, K.; Chen, L.; Chen, Y. Optical Engineering of Uniformly Decorated Graphene Oxide Nanoflakes via in Situ Growth of Silver Nanoparticles with Enhanced Plasmonic Resonance. *ACS Appl. Mater. Interfaces* **2014**, *6* (23), 21069–21077.
- (26) Notarianni, M.; Vernon, K.; Chou, A.; Aljada, M.; Liu, J.; Motta, N. Plasmonic Effect of Gold Nanoparticles in Organic Solar Cells. *Sol. Energy* **2014**, *106*, 23–37.
- (27) Wu, J.-L.; Chen, F.-C.; Hsiao, Y.-S.; Chien, F.-C.; Chen, P.; Kuo, C.-H.; Huang, M. H.; Hsu, C.-S. Surface Plasmonic Effects of Metallic Nanoparticles on the Performance of Polymer Bulk Heterojunction Solar Cells. *ACS Nano* **2011**, *5* (2), 959–967.
- (28) Atwater, H. A.; Polman, A. Plasmonics for Improved Photovoltaic Devices. *Nat. Mater.* **2010**, *9*, 205–213.
- (29) Li, J.; Cushing, S. K.; Meng, F.; Senty, T. R.; Bristow, A. D.; Wu, N. Plasmon-Induced Resonance Energy Transfer for Solar Energy Conversion. *Nat. Photonics* **2015**, *9*, 601–607.
- (30) Xu, P.; Shen, L.; Meng, F.; Zhang, J.; Xie, W.; Yu, W.; Guo, W.; Jia, X.; Ruan, S. The Role of Ag Nanoparticles in Inverted Polymer Solar Cells: Surface Plasmon Resonance and Backscattering Centers. *Appl. Phys. Lett.* **2013**, *102* (12), 123301.
- (31) Luk'yanchuk, B.; Zheludev, N. I.; Maier, S. A.; Halas, N. J.; Nordlander, P.; Giessen, H.; Chong, C. T. The Fano Resonance in Plasmonic Nanostructures and Metamaterials. *Nat. Mater.* **2010**, *9*, 707–715.
- (32) Miroshnichenko, A. E.; Flach, S.; Kivshar, Y. S. Fano Resonances in Nanoscale Structures. *Rev. Mod. Phys.* **2010**, *82* (3), 2257–2298.
- (33) Chen, X.; Zhao, C.; Rothberg, L.; Ng, M.-K. Plasmon Enhancement of Bulk Heterojunction Organic Photovoltaic Devices by Electrode Modification. *Appl. Phys. Lett.* **2008**, *93* (12), 123302.

(34) Yao, M.; Shen, P.; Liu, Y.; Chen, B.; Guo, W.; Ruan, S.; Shen, L. Performance Improvement of Polymer Solar Cells by Surface-Energy-Induced Dual Plasmon Resonance. *ACS Appl. Mater. Interfaces* **2016**, *8* (9), 6183–6189.

(35) Shen, P.; Liu, Y.; Long, Y.; Shen, L.; Kang, B. High-Performance Polymer Solar Cells Enabled by Copper Nanoparticles-Induced Plasmon Resonance Enhancement. *J. Phys. Chem. C* **2016**, *120* (16), 8900–8906.

(36) Gao, J.; Tu, C.; Liang, L.; Zhang, H.; Zhuge, F.; Wu, L.; Cao, H.; Yu, K. Silver Nanoparticles with an Armor Layer Embedded in the Alumina Matrix to Form Nanocermet Thin Films with Sound Thermal Stability. *ACS Appl. Mater. Interfaces* **2014**, *6* (14), 11550–11557.

(37) Jiang, Z. Y.; Chen, X. H.; Lin, X. H.; Jia, X. K.; Wang, J. F.; Pan, L. K.; Huang, S. M.; Zhu, F. R.; Sun, Z. Amazing Stable Open-Circuit Voltage in Perovskite Solar Cells using AgAl Alloy Electrode. *Sol. Energy Mater. Sol. Cells* **2016**, *146*, 35–43.

(38) Luo, Y. D.; Chen, X. H.; Zhang, C. X.; Li, J. J.; Shi, J. H.; Sun, Z.; Wang, Z. C.; Huang, S. M. AgAl Alloy Electrode for Efficient Perovskite Solar Cells. *RSC Adv.* **2015**, *5* (69), 56037–56044.

(39) Chen, S.; Manders, J. R.; Tsang, S.-W.; So, F. Metal Oxides for Interface Engineering in Polymer Solar Cells. *J. Mater. Chem.* **2012**, *22*, 24202–24212.

(40) Li, S.; Liu, P.; Wang, Q. S. Study on the Effect of Surface Modifier on Self-Aggregation Behavior of Ag Nano-Particle. *Appl. Surf. Sci.* **2012**, *263*, 613–618.

(41) Lu, L.; Luo, Z.; Xu, T.; Yu, L. Cooperative Plasmonic Effect of Ag and Au Nanoparticles on Enhancing Performance of Polymer Solar Cells. *Nano Lett.* **2013**, *13* (1), 59–64.

(42) Xu, M.-F.; Zhu, X.-Z.; Shi, X.-B.; Liang, J.; Jin, Y.; Wang, Z.-K.; Liao, L.-S. Plasmon Resonance Enhanced Optical Absorption in Inverted Polymer/Fullerene Solar Cells with Metal Nanoparticle-Doped Solution-Processable TiO<sub>2</sub> Layer. *ACS Appl. Mater. Interfaces* **2013**, *5* (8), 2935–2942.

(43) Kim, J.-Y.; Na, S.-I.; Ha, G.-Y.; Kwon, M.-K.; Park, I.-K.; Lim, J.-H.; Park, S.-J.; Kim, M.-H.; Choi, D.; Min, K. Thermally Stable and Highly Reflective AgAl Alloy for Enhancing Light Extraction Efficiency in GaN Light-Emitting Diodes. *Appl. Phys. Lett.* **2006**, *88* (4), 043507.

(44) Sun, X.; Chen, X.; Zhang, Z.; Sun, Z. Plasmon Based Antireflection Coatings Containing Nanostructured Ag and Silica Medium. *Appl. Surf. Sci.* **2012**, *258* (8), 3785–3788.